4-10-2005

Silicon/Disordered Carbon Nanocomposites for Lithium-Ion Battery Anodes

Z. P. Guo
University of Wollongong, zguo@uow.edu.au

E. Milin
University of Wollongong

J. Z. Wang
University of Wollongong, jiazhao@uow.edu.au

Jun Chen
University of Wollongong, junc@uow.edu.au

Hua-Kun Liu
University of Wollongong, hua@uow.edu.au

Journal of The Electrochemical Society, **152** (11) A2211-A2216 (2005)
0013-4651/2005/152(11)/A2211/6/$7.00 © The Electrochemical Society, Inc.

Silicon/Disordered Carbon Nanocomposites for Lithium-Ion Battery Anodes

Z. P. Guo,[a,z] E. Milin,[a] J. Z. Wang,[a] J. Chen,[b] and H. K. Liu[a,*]

[a]*Institute for Superconducting and Electronic Materials, University of Wollongong, NSW 2500, Australia*
[b]*Intelligent Polymer Research Institute, University of Wollongong, NSW 2522, Australia*

Silicon/disordered carbon (Si–DC) nanocomposites have been synthesized by high-energy ballmilling of Si-sucrose and silicon–polyvinyl alcohol followed by pyrolysis under argon flow. The exact disordered carbon content in the as-prepared Si–DC nanocomposites was determined by thermogravimetric analysis for the first time. Based on the thermogravimetric analysis, X-ray diffraction, Raman, and cyclic voltammetric results, we believe that carbon distribution on the Si particles in Si–DC nanocomposite using PVA as the carbon source is more uniform and has higher efficiency than that using sucrose as the carbon source, under the same preparation conditions. The carbon content and the starting polymers significantly affect the electrochemical performance of the Si–DC nanocomposites. The optimized Si–DC nanocomposite anode demonstrated a reversible capacity of 754 mAh/g within 20 cycles.
 [DOI: 10.1149/1.2051847]

Manuscript submitted April 11, 2005; revised manuscript received July 11, 2005. Available electronically October 4, 2005.

Lithium-ion batteries have become the power source of choice for consumer electronic devices such as cell phones and laptop computers due to their high energy density and long cycle life. In addition, lithium-ion batteries are expected to be a major breakthrough in the hybrid vehicle field. Despite their successful commercial application, further performance improvement of the lithium-ion battery is still required.

Graphitic or graphitization carbons have been used extensively as negative electrode materials for lithium-ion batteries. However, the lithium storage capacity of graphite as associated with its maximum LiC_6 stage[1] is limited to 372 mAh/g. Lithium alloys are also attractive anode candidates because they can incorporate large amounts of lithium. For example, $Li_{4.4}Si$ has a theoretical capacity of 4200 mAh/g. However, lithium alloys are brittle and hence easily pulverized by the large volume change in charge and discharge reactions. The resulting loss of connectivity with the conducting additive particles causes poor cyclability in practice.[2-5] To circumvent this problem, several research efforts have been focused on composites consisting of silicon and carbonaceous materials. For instance, Wilson and Dahn[6] have synthesized nanodispersed silicon in carbon using chemical vapor deposition (CVD). Although the Si–C anodes demonstrated a reversible capacity of 500 mAh/g, it is difficult to control the morphology of Si and C when using the CVD approach. Yoshio et al.[7] prepared carbon-coated silicon by a thermal vapor deposition (TVD) method, and a better cycle life than with the respective silicon has been achieved. Composite produced by mechanically mixing silicon and graphite (or acetylene black) shows high capacity but its cycling is still poor.[8] More recently, research work by many groups has demonstrated that silicon/disordered carbon (DC) composite, obtained by mechanically milling and pyrolyzing organic precursors, such as polyparaphenylene (PPP) or polyvinyl chloride (PVC), in an inert gas atmosphere can reversibly insert Li atoms with a capacity ($>$500 mAh/g) greater than that of graphite (372 mAh/g).[9,10] Although the electrochemical performance is significantly improved compared with the respective silicon electrodes, the silicon-disordered carbon systems still pose some problems, such as a relatively high capacity fading rate and a relatively low capacity contribution from the disordered carbon (386 mAh/g from PVC-based disordered carbon; 451.3 mAh/g from PPP-based disordered carbon). Recently, it was reported that the disordered carbon prepared by pyrolyzing hexa(phenyl)benzene (HPB) demonstrated a stable capacity on the order of 500 mAh/g.[11] Carbon from pyrolyzed sugar under optimal conditions showed a large reversible capacity of 650 mAh/g.[12] Therefore, the optimization of the silicon-disordered carbon system and further improvement of the silicon-disordered carbon concept are necessary.

In this paper, a series of Si–DC samples were synthesized by mechanical milling of Si–sucrose and Si–polyvinyl alcohol (PVA) followed by pyrolysis. Here sucrose was chosen because the DC obtained by sugar pyrolysis shows a large reversible capacity (650 mAh/g);[12] PVA was used because it gives the maximum yield of amorphous carbon compared to other polymers.[13] The disordered carbon content in Si–DC nanocomposites was determined by thermogravimetric analysis (TGA) analysis for the first time. The electrochemical properties of the obtained Si–DC nanocomposites as anodes in lithium-ion cells were systematically evaluated.

Experimental

Preparation and characterization of Si–DC nanocomposites.— Si powder (average particle size 80 nm) and PVA (Aldrich) or sucrose with weight ratios of silicon vs PVA or sucrose from 1:9 to 7:3 were mechanically milled for 10 h to obtain Si–polymer composites with the Si particles coated with polymer. The mixture was then heated at 600°C under argon flow for 2 h at a heating rate of 5°C/min and cooled to room temperature at a natural rate. The as-prepared Si–DC nanocomposites were characterized by scanning electron microscopy (SEM, Leica/Cambridge Stereoscan 440) and X-ray diffraction (XRD) with Cu Kα radiation (MO3xHF22, MacScience, Japan). Raman spectroscopy was used to monitor the variations in the carbon using a JOBIN YVON HR800 Confocal Raman system with 632.8-nm diode laser excitation on a 300 lines/mm grating at room temperature. The precise DC concentration in Si–DC nanocomposites was determined using TGA/differential thermal analysis (DTA) via a Setaram TGA/DTA apparatus. The samples were heated in an alumina crucible from room temperature to 900°C at 10°C min^{-1} in air.

Electrochemical characterization.— Teflon-type and coin cells were assembled for electrochemical characterization of Si–DC nanocomposite electrodes. The testing electrodes were made by dispersing 80 wt % active materials, 15 wt % carbon black, and 5 wt % polyvinylidene fluoride (PVDF) binder in dimethyl phthalate solvent to form a slurry. The slurry was then spread onto a copper foil and dried in a vacuum oven. The electrodes were Φ 12-mm disks, and the weight of the electrodes was about 1.5 mg. The cells were assembled in an argon-filled glove box (MBraun, Unilab, USA). The electrolyte was 1 M $LiPF_6$ in a mixture of ethylene carbonate (EC) and dimethyl carbonate (DMC) (1:1 by volume, provided by Merck KgaA, Germany). The cells were galvanostatically charged and discharged at 50 mA/g over the voltage range 0.02–1.2 V vs Li/Li^+.

* Electrochemical Society Active Member.
z E-mail: zguo@uow.edu.au

Cyclic voltammetry (CV) measurements were carried out on a potentiostat (model M362, EG&G PAR, USA) at a scanning rate of 0.5 mV/s.

Results and Discussion

Determination of carbon content in the Si–DC nanocomposites.— Although there have been some investigations on Si–C composite anodes for lithium-ion batteries,[6-10] the exact content of carbon in the Si–C composites or the detailed structure and morphology of the carbon have not been addressed. It is well known that the content, structure, and morphology of polymer pyrolyzed carbon are affected by the sintering temperature, gas flow rate, polymer precursors, etc.[12] In order to optimize the Si–C composites, it is really necessary to determine the exact carbon content in Si/C composites.

When heated in air, carbon in Si/DC nanocomposites is burnt and releases gas (mainly CO_2, constituting a weight loss), while Si in the nanocomposites is oxidized and SiO_2 is formed (weight gain). Therefore, it is hard to identify the weight loss region where carbon is burnt. A calibration curve is necessary to calculate the carbon ratio in Si/DC nanocomposites. In order to obtain the calibration curves, TGA was carried out on Si/C mixtures with certain known Si/C ratios (with the carbon obtained by pyrolyzing sucrose or PVA under the same conditions). The TGA curves and calculated calibration curves are shown in Fig. 1. Then TGA on as-prepared Si/DC nanocomposites was conducted. The value of the mass loss percentage was taken at the lowest point of the TGA curves and converted into the real content (Table I) of carbon in the Si/DC nanocomposite according to the equation of the fitted curve in Fig. 1b. The carbon concentrations obtained were significantly below the levels originally targeted. For example, when we added enough PVA to produce 49.1% w/w C (10 wt % Si/90 wt % PVA), we actually achieved 28.6% w/w C in the final powder due to carbon burnt out in the sintering stages of Si–DC synthesis.

Structure and morphology analysis of Si–DC nanocomposites.— Figure 2 shows XRD patterns of high-carbon-content Si–DC nanocomposites from 90% PVA/10% Si and 80% sucrose/20% Si, respectively. (Discussion is focused on the Si–DC nanocomposites from 90% PVA/10% Si and 80% sucrose/20% Si because their real carbon contents are similar, i.e., 28.6 and 28.9%.) The XRD pattern of the bare Si sample is also presented for comparison. No peaks corresponding to carbon can be seen, which suggests that the carbon obtained by pyrolyzing sugar or PVA is amorphous. The peaks due to Si diffractions can be clearly observed, and the intensity of the Bragg peaks of silicon for Si–DC nanocomposites is higher than that of the bare Si. In addition, although both Si–DC nanocomposites were obtained at the same temperature (600°C), the intensity of the Si Bragg peaks for Si–DC from 80% sucrose/20% Si is slightly higher, indicating that the size of the silicon crystallites is bigger compared to that of Si–DC from 90% PVA/Si. The crystallite size of Si was calculated using the Scherrer equation,[14] and the calculated crystallite sizes of Si in the bare Si, Si–DC from 90% PVA/10% Si, and Si–DC from 80% sucrose/20% Si are 11, 17, and 59 nm, respectively. A possible interpretation for this phenomenon is the amount and rate of pyrolysis gases (especially CO_2) released from sucrose and PVA are different. For the Si–DC from 90% PVA/Si, more pyrolysis gases are released based on the carbon content analysis results (Table I). The gases are released very fast, which efficiently prevents the growth of silicon crystallites. No SiC phase peak was found in samples produced under the present pyrolyzing conditions. Wilson and Dahn reported that SiC is formed in carbons containing nanodispersed Si atoms if the content of silicon exceeds 11 atom %.[6] Wilson et al. utilized gases as the starting materials, whereas we used polymers as the carbon source and adopted nano-Si powder as a starting material. This may be one of the reasons why no crystalline SiC was produced.

Laser Raman spectroscopy gives information about the vibrations of atoms in crystals and molecules and can be used as a complementary tool to XRD. Figure 3 shows the Raman spectra of Si–DC nanocomposites. The Raman spectra of graphite and the bare disordered carbon pyrolyzed from sucrose are also shown for comparison. Two main peaks were observed at around 1350 and 1580 cm^{-1}, which are designated as the D band and the G band,[15] respectively. The G band is associated with the allowed E_{2g} optical modes of the Brillouin zone center of the crystalline graphite, while

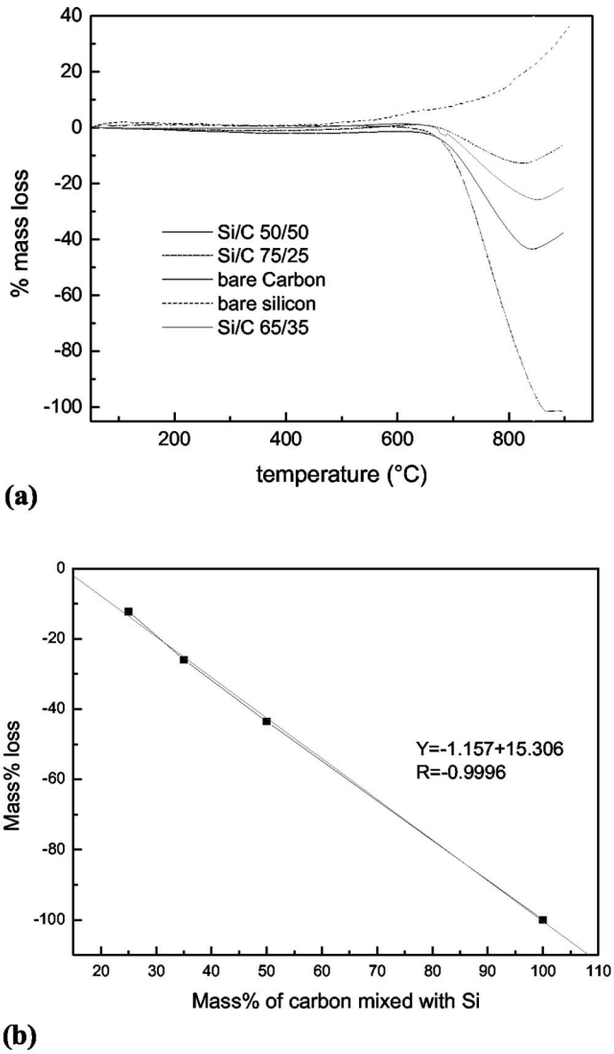

Figure 1. (a) TGA curves of Si/C mixtures with different Si/C ratios and (b) the calibration curve worked out from the TGA curves above.

Table I. Theoretical and real carbon concentrations in Si/DC nanocomposites synthesized from different carbon sources.

Samples	Theoretical (targeted) weight % of carbon	Weight % of carbon	Mass loss % of carbon (%)
20 wt % Si/80 wt % sucrose	33.7	28.9	14.24
33 wt % Si/66 wt % sucrose	27.8	23.7	14.74
70 wt % Si/30 wt % sucrose	12.6	10.3	18.25
10 wt % Si/90 wt % PVA	49.1	28.6	41.75
20 wt % Si/80 wt % PVA	43.6	20.4	53.21
50 wt % Si/50 wt % PVA	27.3	7.5	72.52

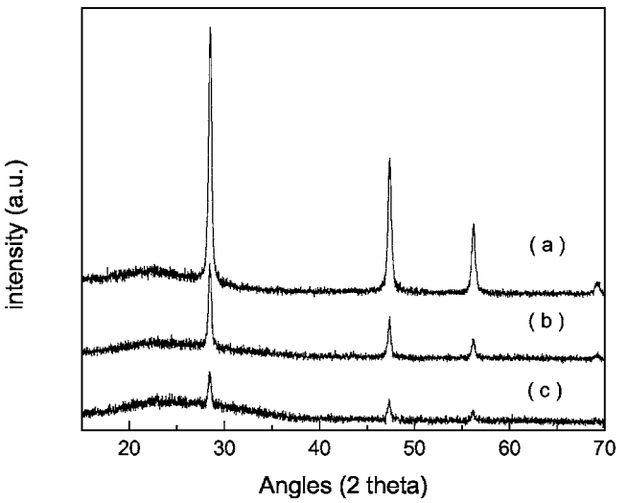

Figure 2. XRD patterns of (a) Si–DC nanocomposite pyrolyzed from 20 wt % Si/80 wt % sucrose; (b) Si–DC nanocomposite pyrolyzed from 10 wt % Si/90 wt % PVA; and (c) bare Si sample.

the D band is attributed to disorder-allowed phonon modes, which become Raman active as a result of lack of long-range order in amorphous graphitic materials.[16] Another small Raman band at 1620 cm^{-1} is also observed, which is the upward shift of peak G due to disorganized carbon.[17] The relative intensity ratio of the D and G bands, I_D/I_G, is known to depend on the structural characteristics of carbon.[18] The ratio can give information about the perfection of the graphite layer structure, reflecting the properties of the edge plane or boundary of the graphite crystal faces. As the I_D/I_G ratio increases, the defect structure increases and the degree of graphitization becomes less.[19] All the I_D/I_G ratios are listed in Table II. The I_D/I_G ratio of carbon produced by pyrolyzing sugar is almost four times higher than that of graphite, suggesting high disorder of the carbon sample. For the Si–DC nanocomposites, only one Raman band at about 520 cm^{-1}, corresponding to a Si lattice vibration, is observed, except for the three peaks assigned to disordered carbon, indicating that the carbon in Si–DC nanocomposites is still disordered carbon.

SEM images of Si–DC nanocomposites compared with disordered carbon pyrolyzed from sucrose are shown in Fig. 4. Note the

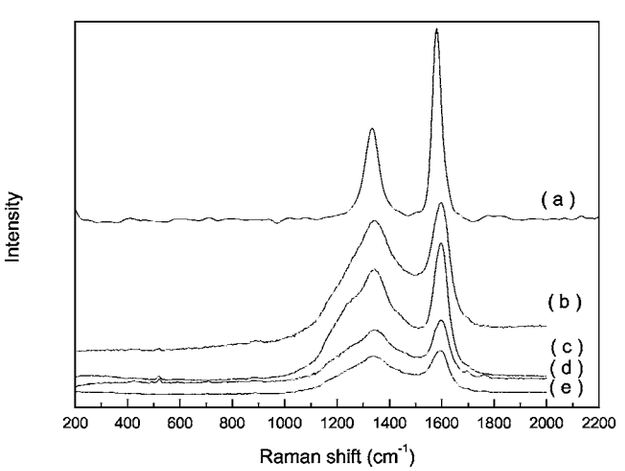

Figure 3. Raman spectra of Si–DC nanocomposites from (a) graphite; (b) 67% sucrose/33% Si; (c) 80% PVA/20% Si; (d) 80% sucrose/20% Si; and (e) disordered carbon produced by pyrolyzing sucrose.

Table II. The relative intensity ratio of the D and G bands (I_D/I_G) obtained from experimental spectra shown in Fig. 3.

Samples	I_D/I_G
Graphite	0.53
67% sucrose/33% Si	2.46
80% PVA/20% Si	2.38
80% sucrose/20% Si	2.35
Disordered carbon produced by pyrolyzing sucrose	2.41

change in powder morphology depends on the polymer carbon source and its ratio. For bare disordered carbon (Fig. 4c), a nonuniform morphology, comprising differently shaped flakes, is shown. Compared with Si starting powder, the particles of all Si–DC nanocomposites become dense and less porous, especially for the Si–DC nanocomposite from 80% sucrose/20% Si. This result is in good agreement with results obtained from XRD. EDX mapping of the different elements was conducted to analyze the distribution of the species within the agglomerated particles (Fig. 5). The bright spots correspond to the presence of each element. Based on the EDX elemental maps, C in the Si–DC nanocomposite from 80% sucrose/20% Si is not completely well-distributed, while the distribution of C in the Si–DC powder from 90% PVA/10% Si is more homogeneous. These indicate that a uniform distribution of C on all the particles is not easily achieved by pyrolyzing sucrose, but a more uniform carbon coating on silicon particles can be achieved by pyrolyzing PVA.

Electrochemical performance of Si–DC nanocomposites.— CVs of Si–DC nanocomposite electrodes in lithium-ion cells, in which a lithium foil was used as the counter electrode and reference electrode, are shown in Fig. 6. The three-electrode CV cells were cycled at a scan rate of 0.5 mV/s. For the Si–DC nanocomposite from 90% PVA/10% Si, the irreversible peak of electrolyte decomposition ranging from 0.5 to 1.1 V vs Li/Li^+ can hardly be seen, which implies that the electrolyte decomposition on the surface is suppressed to a small extent by the carbon coating.[7] By contrast, the irreversible peak corresponding to the electrolyte decomposition is clearly observed in CVs of both Si–DC nanocomposite electrodes from 50% PVA/50% Si and 80% sucrose/20% Si. This may suggest that the Si particles in Si–DC nanocomposites from 50% PVA/50% Si and 80% sucrose/20% Si were not effectively covered by the carbon coating. From the TGA results, the carbon content in Si–DC from 50% PVA/50% Si is only 7.5%, which may not be high enough to fully cover the Si particles. For the Si–DC nanocomposites from 80% sucrose/20% Si, although the carbon concentration is 28.9%, slightly higher than that of 90% PVA/10% Si (28.6%), the irreversible peak from 0.5 to 1.5 V in the first cycle still existed, implying that the pyrolyzed carbon is not uniformly decomposed on the surface of the silicon. By comparison of the CVs of all the electrodes, it was found that the peak shapes were slightly different. For the Si–DC nanocomposites from 90% PVA/10% Si and 80% sucrose/20% Si, there are two anodic peaks that can be clearly seen at about 0.36 and 0.54 V vs Li/Li^+, respectively. A shoulder peak at about 0.2 V vs Li/Li^+ can also be observed. These peaks originate from the phase transitions between $Li_{4.4}Si$, $Li_{2.33}Si$, $Li_{1.71}Si$, and Si, respectively.[4] However, for the 50% PVA/50% Si sample, the two anodic peaks at about 0.36 and 0.54 V vs Li/Li^+ are not clearly split. Instead, the anodic current begins to rise up at a slope from 0.3 V vs Li/Li^+ and merges with the anodic peak at 0.54 V, which may be caused by the large polarization of the electrode. These phenomena suggest that a high content of pyrolyzed carbon could effectively decrease the inner resistance of silicon electrodes due to the high conductivity of the carbon, thereby decreasing the polarization of the silicon electrodes.

The 1st, 3rd, 5th, and 10th charge/discharge curves of Si–DC nanocomposite electrodes from 80% sucrose/20% Si and 90% PVA/10% Si are shown in Fig. 7. In the first cycle, the dis-

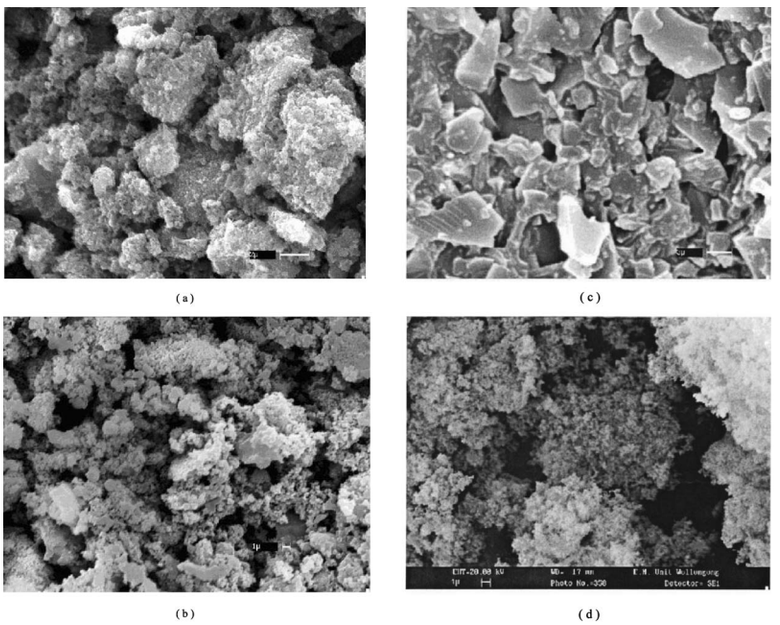

Figure 4. SEM images of (a) Si–DC nanocomposite pyrolyzed from 90% PVA/Si; (b) Si–DC from 80% sucrose/Si; (c) disordered carbon obtained by pyrolyzing sucrose; and (d) Si starting materials.

charge capacities (intercalation of lithium into the Si-based electrode) were 1165 and 1254 mAh/g, while the charge capacities (deintercalation from the Si-based electrode) were 935 and 841 mAh/g for Si–DC nanocomposite electrodes from 90% PVA/10% Si and 80% sucrose/20% Si, respectively. Thus, the coulombic efficiency in the first cycle for Si–DC nanocomposite electrodes from 90% PVA/10% Si was 80.3%, while it was much lower for Si–DC nanocomposite electrodes from 80% sucrose/20% Si (67.1%). This result is consistent with that from CV and further demonstrates that the carbon coating achieved by using PVA as the carbon source on Si particles is more uniform and produced more efficiently than that produced by using sucrose as the carbon source. In addition, a potential plateau at about 0.4 V can be observed in the first few cycles in the charge curves; however, it gradually becomes more sloped and shorter during charge/discharge cycling, which indicates that some irreversible structural changes have occurred and the amount of Li extraction from silicon in the Si–DC nanocomposite electrodes has decreased.

The reversible capacities as a function of cycle number are compared in Fig. 8. The reversible capacity is up to 754 mAh/g after 20 charge/discharge cycles, which suggests that the nanocomposite materials are promising as anode materials for Li-ion batteries. From Fig. 8, we can also see that the cycle life decreases in order as follows:

Si–DC from 90% PVA/10% Si > Si–DC from 80% PVA/20% Si >Si–DC from 80% sucrose/20% Si >Si–DC from 67% sucrose/33% Si > Si–DC from 50% PVA/50% Si >Si–DC from 30% sucrose/70% Si

In Si–DC nanocomposites, the nanosized silicon particles are separated and coated by disordered carbon, which could not only suppress the decomposition of electrolytes on the surface of Si-based electrode, but also provide integral and continuous electric contact networks around Si particles even when they are slightly expanded after lithium insertion.[7] It is obvious that the carbon content and starting polymer used significantly affect the capacity and cycling behavior of Si–DC nanocomposite electrodes. We believe that the electrochemical performance of Si–DC nanocomposites can be further optimized through tuning the material processing. A more detailed study of the effects of preparation conditions, such as mill design, sintering temperature and time, gas flow rate, heating rate, and starting polymer, on electrochemical performance is in progress in our laboratory.

Conclusions

Si–DC nanocomposites have been synthesized by mechanical milling of Si–sucrose and Si–PVA followed by pyrolysis under argon flow. The Si–DC nanocomposite from 90% PVA/10% Si shows

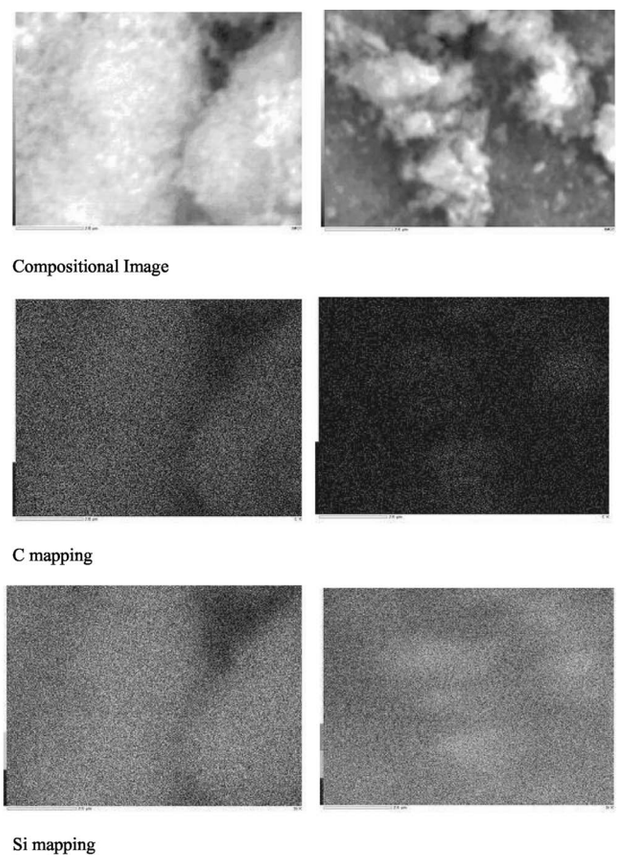

Figure 5. EDX mapping of Si–DC nanocomposites by pyrolyzing 90% PVA/10% Si (left) and 80% sucrose/20% Si (right).

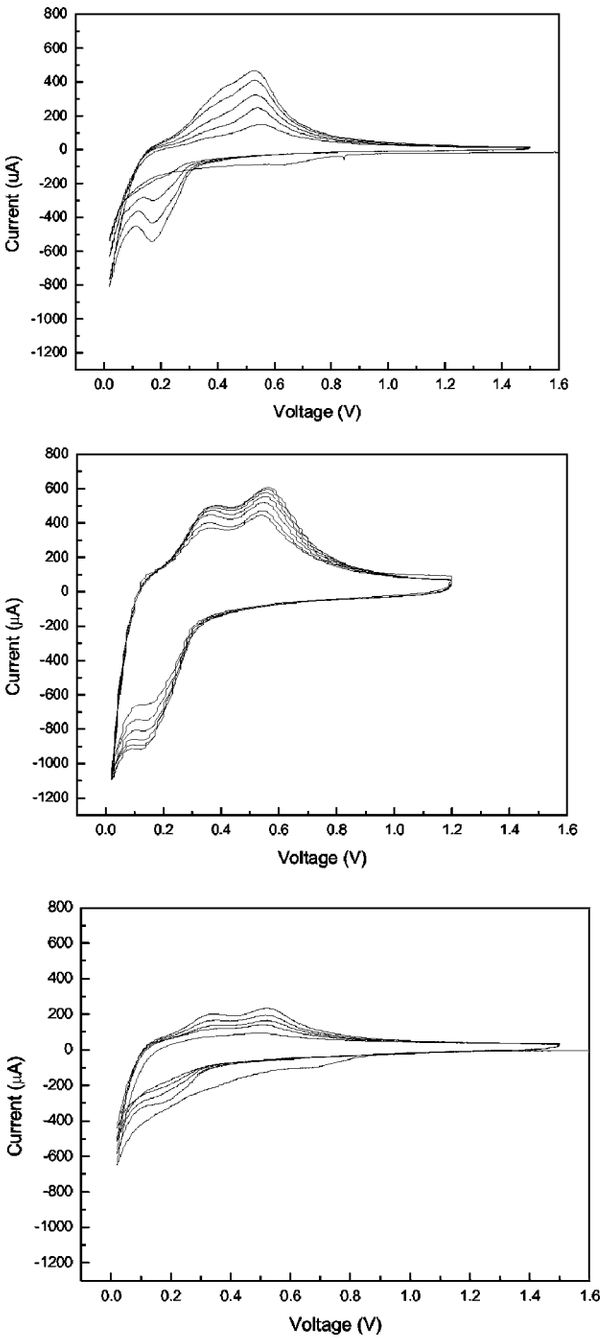

Figure 6. CVs of Si–DC nanocomposites from 50% PVA/50% Si (upper); 90% PVA/10% Si (middle); and 80% sucrose/20% Si (lower), respectively.

a high reversible capacity of 754 mAh/g within 20 cycles and a high initial coulombic efficiency of 80.3%. The carbon content and starting polymer used significantly affect the capacity and cycling behavior of Si–DC nanocomposite electrodes. The exact disordered carbon content in the as-prepared Si–DC nanocomposites was determined by TGA for the first time. TGA, XRD, Raman, and CV results demonstrated that the carbon distribution on the Si particles in Si–DC nanocomposite using PVA as the carbon source is more uniform than that using sucrose as the carbon source under the same preparation conditions. Carbon analysis using TGA appears to be a good way to investigate carbon-containing composites. We believe that this approach to analysis warrants significant further work.

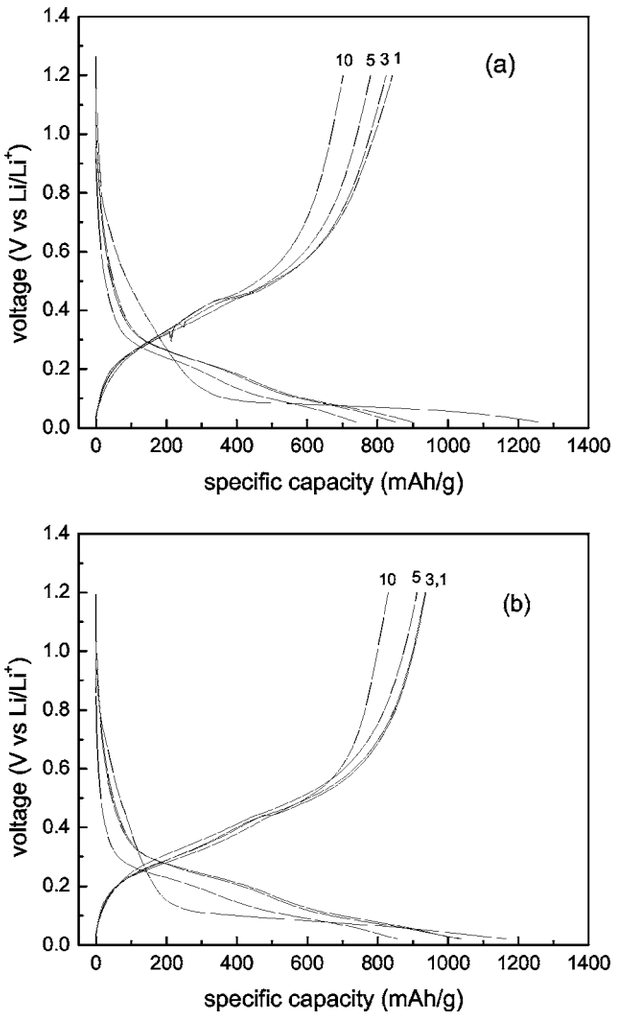

Figure 7. The 1st, 3r, 5th, and 10th charging/discharging curves for the Si/DC nanocomposites obtained by pyrolyzing (a) 80% sucrose/20% Si and (b) 90% PVA/10% Si.

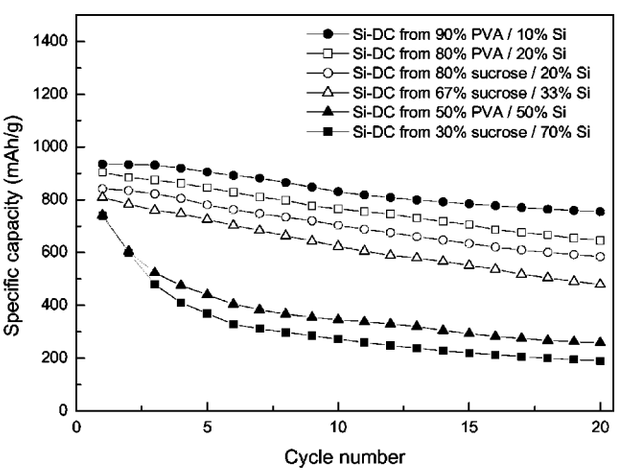

Figure 8. Cycle life behavior of Si–DC nanocomposites. Current density 50 mA/g.

Acknowledgments

The authors would like to thank Dr. K. Konstantinov for his help with the SEM measurements. Financial support from the Australian Research Council is gratefully acknowledged.

The University of Wollongong assisted in meeting the publication costs of this article.

References

1. J. R. Dahn, T. Zheng, Y. H. Liu, and J. S. Xue, *Science*, **270**, 590 (1995).
2. M. Winter and J. O. Besenhard, *Electrochim. Acta*, **45**, 31 (1999).
3. Sanyo Electric, U.S. Pat. 4,820,599 (1989).
4. B. A. Boukamp, G. C. Lesh, and R. A. Huggins, *J. Electrochem. Soc.*, **128**, 725 (1981).
5. O. Mao and J. R. Dahn, *J. Electrochem. Soc.*, **146**, 405 (1999).
6. A. M. Wilson and J. R. Dahn, *J. Electrochem. Soc.*, **142**, 326 (1995).
7. M. Yoshio, H. Wang, K. Fukuda, T. Umeno, N. Dimov, and Z. Ogumi, *J. Electrochem. Soc.*, **149**, 1598 (2002).
8. H. Li, X. J. Huang, L. Q. Chen, G. W. Zhou, and Y. Liang, *Electrochem. Solid-State Lett.*, **2**, 547 (1999).
9. Y. Liu, K. Hanai, J. Yang, N. Imanishi, A. Hirano, and Y. Takeda, *Solid State Ionics*, **168**, 61 (2004).
10. X. Zhang, P. K. Patil, C. Wang, A. J. Appleby, F. E. Little, and D. L. Cocke, *J. Power Sources*, **125**, 206 (2004).
11. F. Bonino, S. Brutti, P. Reale, B. Scrosati, L. Gherghel, J. Wu, and K. Mullen, *Adv. Mater. (Weinheim, Ger.)*, **17**, 743 (2005).
12. W. Xing, J. S. Xue, and J. R. Dahn, *J. Electrochem. Soc.*, **143**, 3046 (1996).
13. N. Maksimova and O. P. Krivoruchko, *Chem. Eng. Sci.*, **54**, 4351 (1999).
14. J. Piscoe and B. E. Warren, *J. Appl. Phys.*, **13**, 364 (1942).
15. M. Yoshikawa, G. Katagiri, H. Ishida, and A. Ishitani, *Solid State Commun.*, **66**, 1177 (1988).
16. F. Tuinstra and J. L. Koening, *J. Chem. Phys.*, **53**, 1126 (1970).
17. N. Wada, P. J. Gaczi, and S. A. Solin, *J. Non-Cryst. Solids*, **35**, 543 (1980).
18. J. Kastner, T. Pichler, and H. Kuzmany, *Chem. Phys. Lett.*, **221**, 53 (1994).
19. F. X. Wang, X. P. Gao, Z. W. Lu, S. H. Ye, J. Q. Qu, F. Wu, H. T. Yuan, and D. Y. Song, *J. Alloys Compd.*, **370**, 326 (2004).